



Electrochemical charge of silica surfaces at high ionic strength in narrow channels

Moran Wang^{a,b,*}, André Revil^{c,d}

^a Computational Earth Sciences Group (EES-16), Earth and Environmental Sciences Division, Los Alamos National Laboratory, Los Alamos, NM 87545, USA

^b Center of Nonlinear Studies, Theoretical Division, Los Alamos National Laboratory, Los Alamos, NM 87545, USA

^c Department of Geophysics, Colorado School of Mines, Golden, CO 80401, USA

^d CNRS-UMR 5559-LGIT, Université de Savoie, Equipe volcan, 73376 Le-Bourget-du-Lac, France

ARTICLE INFO

Article history:

Received 8 October 2009

Accepted 18 November 2009

Available online 23 November 2009

Keywords:

Electrical triple-layer

Electrochemical charge

Charge regulation

High ionic strength

ABSTRACT

We present a theoretical framework to calculate the electrochemical charge on silica surfaces in contact with high-ionic-strength solutions in narrow channels. Analytical results indicate that the contribution of the adsorbed metal cations to the total surface charge is not negligible when the salinity is larger than 1 mM. The electrical triple-layer model is proved much better than other models for high ionic strength. The charge regulation caused by the double-layer overlap in narrow channels will reduce the surface charge density but increase the zeta potential on silica surfaces.

Published by Elsevier Inc.

1. Introduction

Electrokinetic transport in microfluidics and nanofluidics has been an emerging field of interest because of its potential capabilities for controlling and manipulating fluids and inclusions (particles and ions) exquisitely [1–5], and of its potential applications in biochemical analysis [6–8] and energy conversion systems [9–12]. The electrokinetic transport in micro- or nano-scale channels has two important features compared with that in large channels: (1) the salt concentration is often high (>1 mM), and (2) the electrical diffuse layers may often interact with each other. Many efforts have been reported in recent years for analysis and modeling of such a multiphysiochemical transport process using the continuum-based [2,4,7,9,13–16], molecular-based [17–20], or mesoscopic methods [21,22]; however, it is still a big challenge for accurate predictions because of its complexity.

The difficulty comes mainly from two aspects. The first is the electrochemical charge determination at solid–liquid interfaces. In most of the previous modeling studies, either constant charge density [7,9,17–21] or constant zeta potential [15,22] was employed as the electric boundary conditions at surfaces. However, as well known, the nonmetal surfaces are generally ionized in aqueous solutions by physical and chemical adsorptions of ions, and the surface charge density results from an equilibrium

between counter ions at the surfaces and free ions in the bulk electrolyte. Behrens and Grier [23] proposed a Basic Stern (BS) model which provided a relationship between the surface charge and the bulk electrolyte solution properties, and this chemical equilibrium model has been used for modeling of electrokinetic transport in microfluidic or nanofluidic channels [4,14]. The BS model is simple in mathematics; however, it considers only the silica dissociation with water molecules and ignores the contributions from the salt ions. As a result, the BS model is only available to very dilute solutions [23]. To involve the contribution from the salt–ion adsorption to the surface charge on mineral surfaces, an electrical triple-layer (ETL) model was first proposed by Davis et al. [24,25], developed by Kitamura et al. [26], and elaborated by Leroy and coworkers [27,28]. Furthermore, a more complex four-layer model was proposed to distinguish the sizes of anions and cations adsorbed at the electrolyte/oxide interfaces [29,30]. The ETL model has been employed for analysis of electrokinetic transport in geophysics and geochemistry [27,28,31]; however, to the best knowledge of the authors, neither the triple-layer model nor the four-layer model have been adopted for predictions of electrokinetic transport in microfluidics or nanofluidics. The second difficulty lies in the charge regulation by the electrical diffuse-layer overlap. When the surface separation of a microchannel is comparable to or smaller than the Debye screening length, the electrical diffuse-layer overlap will cause the charge regulation both in the “bulk” solution in the channel and on the surfaces. Behrens and Grier [23] proposed a method to cover the charge regulation of anionic surfaces by solving the nonlinear Poisson–Boltzmann equation using the Jacobian elliptic functions. However, this method has a good numerical convergence only for a very narrow region

* Corresponding author. Address: Computational Earth Sciences Group (EES-16), Earth and Environmental Sciences Division, Los Alamos National Laboratory, Los Alamos, NM 87545, USA.

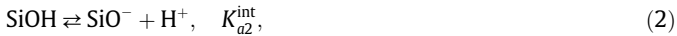
E-mail addresses: mwang@lanl.gov, moralwang@jhu.edu (M. Wang).

of surface separation [23] and can hardly be extended for the ETL model. Up to now no charge regulation analysis has been found subject to the ETL model or the four-layer model.

In this work, we focus on the electrochemical charge for silica surfaces, which are among the most popularly used materials in microfluidics and nanofluidics [2,23], at high ionic concentrations (1 mM to 1 M). In the following sections, the electrical triple-layer model is first introduced and validated for determinations of charge density and zeta potential on silica surfaces for various salt electrolyte solutions at high ionic concentrations. A charge regulation analysis is then performed subject to the ETL model when the electrical diffuse-layer overlap occurs. The electrochemical charge in micro- and nanochannels is therefore discussed.

2. Electrical triple-layer model

Let us consider a silica surface in contact with a binary symmetric aqueous electrolyte such as the NaCl or KCl solution for the simplicity of presentation. The silica surface acquires charges by chemical adsorptions of ions in the solution, and the surface charge strongly depends on the local environmental factors such as pH, ionic strength, and temperature. Fig. 1 sketches the adsorption effect on the ions distribution, based on which the electrical triple-layer (ETL) model is established [24,25,27,28]. In the pH range 3–9, the typical chemical reactions of surface adsorption at the silica surface can be written as



and



where K_{a1}^{int} , K_{a2}^{int} , K_M^{int} , and K_A^{int} are the associated equilibrium constants for the reactions, respectively. More reaction equations can be easily added for multicomponent electrolyte similar to Eqs. (3) and (4) [27,28] or Eq. (3) can be adapted for a multivalent cations [26]; therefore, the present model is not limited to the binary salt. The protonation of surface siloxane groups is extremely low so that

they are generally considered inert [32]. The silanol group may become positively charged by accepting protons under very acidic solutions (pH < 3), and the silica significantly dissolves into silicate ions HSO_3^- in basic solution (pH > 9); therefore, the present ETL model is restricted to the pH range 3–9.

Note that in Fig. 1 the adsorption of anion A^- by the SiOH_2^+ sites is sketched by a dashed-line connection because this reaction rate is extremely low at the pH range 3–9 and can only be considerable when pH < pH(pzc), where pH(pzc) denotes the pH at the point of zero charge of surfaces. For silica surfaces, pH(pzc) is around 2–3 and has a relationship with K_{a1}^{int} and K_{a2}^{int} :

$$\text{pH}(\text{pzc}) = \frac{1}{2} (\log K_{a1}^{\text{int}} + \log K_{a2}^{\text{int}}). \quad (5)$$

In the present work, we have pH(pzc) \approx 2.5 [33]. Once the adsorption rate of anion Cl^- is not negligible, the four-layer model may be more suitable to describe the ions distributions because of the size difference between cations and anions [30].

Based on the law of mass action, the reaction equilibrium constants for the chemical adsorptions can be expressed as

$$K_{a1}^{\text{int}} = \frac{\sigma_{\text{SiOH}}}{\sigma_{\text{SiOH}_2^+}} C_{\text{H}^+}^{\text{b}} \exp\left(-\frac{e\psi_o}{kT}\right), \quad (6)$$

$$K_{a2}^{\text{int}} = \frac{\sigma_{\text{SiO}^-}}{\sigma_{\text{SiOH}}} C_{\text{H}^+}^{\text{b}} \exp\left(-\frac{e\psi_o}{kT}\right), \quad (7)$$

$$K_M^{\text{int}} = \frac{\sigma_{\text{SiOM}}}{\sigma_{\text{SiO}^-}} \frac{1}{C_{\text{M}^+}^{\text{b}}} \exp\left(-\frac{e\psi_\beta}{kT}\right), \quad (8)$$

where σ denotes the surface charge density, C^{b} the bulk molar concentration of ions (in M), ψ the electric potential, e the electron charge, k the Boltzmann constant, and T the temperature.

The continuity equation for the surface charge density yields

$$e\Gamma_0 = \sigma_{\text{SiOH}} + \sigma_{\text{SiO}^-} + \sigma_{\text{SiOH}_2^+} + \sigma_{\text{SiOM}}, \quad (9)$$

where Γ_0 is the total surface site density (in sites/m²). The ETL model in Fig. 1 yields the surface charge density at the silica surface, Q_o , as

$$Q_o = \sigma_{\text{SiOH}_2^+} - \sigma_{\text{SiO}^-} - \sigma_{\text{SiOM}}, \quad (10)$$

and the surface charge density of the Stern layer, Q_β , as

$$Q_\beta = \sigma_{\text{SiOM}}. \quad (11)$$

The site charge density σ_{SiOM} contributes to Q_o because the site SiOM is actually $\text{SiO}^- - \text{M}^+$ with SiO^- located on the silica surface and M^+ located in the Stern layer, as shown in Fig. 1.

For an insulated surface, the equivalent surface charge of the diffuse layer, Q_d , can be calculated using the classical Gouy–Chapman model. Especially for a symmetric monovalent electrolyte, it has

$$Q_d = -\sqrt{8\varepsilon kT n_s^{\text{b}}} \sinh\left(\frac{e\psi_d}{2kT}\right), \quad (12)$$

where ε is the permittivity of the electrolyte, and n_s^{b} is the bulk number density of salt (in m⁻³) which is related to the bulk ionic concentration as

$$n_s^{\text{b}} = 1000N_A(C_{\text{M}^+}^{\text{b}} + C_{\text{H}^+}^{\text{b}}), \quad (13)$$

with N_A representing the Avogadro constant and $(C_{\text{M}^+}^{\text{b}} + C_{\text{H}^+}^{\text{b}})$ the counterions bulk molar concentration (in M).

The global electroneutrality within the triple layers yields

$$Q_o + Q_\beta + Q_d = 0. \quad (14)$$

The electric potentials of the triple layers are related to the charge densities by

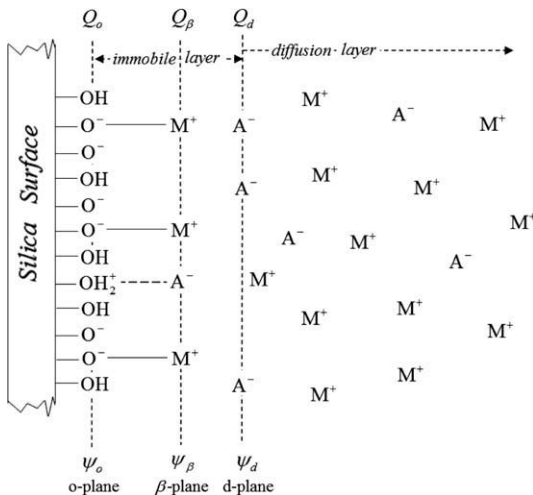


Fig. 1. Sketch of the electrical triple-layer model [24,25,27,28]. The symbol M represents the metal cations (e.g., Na⁺ or K⁺) and A the anions (e.g., Cl⁻). Q_o and ψ_o are the surface charge density and the electrical potential of the silica surface, Q_β and ψ_β are the surface charge density and the electrical potential of the Stern layer, and Q_d and ψ_d are the equivalent surface charge density and the electrical potential (zeta potential, ζ) of the diffuse layer.

$$\psi_o - \psi_\beta = Q_o/C_1, \quad (15)$$

$$\psi_\beta - \psi_d = -Q_d/C_2, \quad (16)$$

where C_1 and C_2 (in F/m^2) are the integral electrical capacities of the inner and outer parts of the Stern layer, respectively, assuming constant in the regions between planes [30].

Eqs. (6)–(16) yield the coupled nonlinear equations for the charge densities and electric potentials of the triple layers ($Q_o, Q_\beta, Q_d, \psi_o, \psi_\beta, \psi_d$) when the other parameters are given. The surface charge density and the zeta potential are therefore solved out using the Newton method numerically by Matlab [34].

To validate the ETL model, we compare the predictions with the available experimental data from the literatures [26,35]. Fig. 2 shows the predicted surface charge density and zeta potential on silica surfaces versus the pH value of NaCl solutions. The lines are the ETL predictions, and the symbols are the experimental data. The parameters in the ETL model are $\Gamma^0 = 5$ sites/ nm^2 , $K_{a2}^{int} = 10^{-6.73}$, $K_M^{int} = 10^{-0.25}$, $C_1 = 1.07$ F/ m^2 , and $C_2 = 0.2$ F/ m^2 . The temperature is $T = 298$ K. The results show that the ETL predictions agree well with the experimental data from different researchers [26,35] for ionic concentrations at 10^{-3} – 10^{-1} M, which validates the ETL model for high salt concentrations.

This mathematical framework presented by Eqs. (6)–(16) is also suitable directly to other kinds of monovalent salts interacting with silica surfaces. Table 1 lists the parameters of the ETL model for four most popular salts. However, the present ETL model is not limited to monovalent salts. For multivalence salts, the chemical reaction equilibrium Eqs. (3) and (4) are little different [26]. Besides, Eq. (12) may have a more complex form.

As we stated before, we introduce the ETL model just to overcome the difficulties from high salinities for other simple models, such as the popular Basic Stern model. Fig. 3a compares the theoretical predictions using the ETL model and the Basic Stern model with the measured zeta potentials by Gaudin and Fuerstenau [36] at high salinity range. The result indicates that the ETL model agrees much better than the Basic Stern model with the experimental data. The reason lies mainly in the contribution of the adsorbed metal cations on silica surfaces, which is taken into account in the ETL model (shown in Eq. (3)) but ignored in the Basic Stern model. Such a contribution increases sharply with the salinity. Fig. 3b shows the proportion of surface charge by the adsorbed metal cations to the total surface charge (σ_{SiOM}/Q_o) as a function of the NaCl salinity. If we define 3% as a critical value that the contribution is not negligible, we find that the corresponding

Table 1
Parameters in the ETL model for silica surfaces.^a

Electrolyte solution	LiCl	NaCl	KCl	CsCl
C_1	2.21 ± 0.46	1.07 ± 0.13	1.16 ± 0.14	1.84 ± 0.23
$\text{Log } K_{a2}^{int}$	-6.74 ± 0.12	-6.73 ± 0.11	-6.64 ± 0.20	-6.56 ± 0.12
$\text{Log } K_M^{int}$	-0.35 ± 0.24	-0.25 ± 0.20	0.06 ± 0.30	-0.01 ± 0.20

^a The parameters are obtained through fitting the experimental data for given $\Gamma_1 = 5$ sites/ nm^2 and $C_2 = 0.20$ F/ m^2 . The parameters are best fit for the most popular amorphous silica [26].

salinity is around 10^{-3} M. This result indicates that the contribution from the adsorbed metal cations to the total surface charge is not negligible when the NaCl salinity is larger than 1 mM. The Basic Stern model and other models in which the adsorption of metal cations is not considered are only valid for low ionic strength ($C_s^\infty < 1$ mM). For high ionic strength ($C_s^\infty > 1$ mM), the ETL model is a better choice.

After validation, the ETL model is employed to investigate the surface charge density and zeta potential varieties on silica surfaces with the ionic strength and the pH of electrolyte solutions. The surface charge densities and zeta potentials changing with pH values for three different ionic strengths are shown in Fig. 2. Both the surface charge density and the absolute value of zeta potential increase nonlinearly with the pH value of solutions if the ionic concentration is given. Fig. 4a and b shows the surface charge density and zeta potential as a function of salinity, respectively, for three pH values. The surface charge density increases with the salinity, while the absolute value of zeta potential decreases with the salinity, if the pH of solution is given. When the surface charge density versus salinity is plotted into a log–log frame system, the curves are almost straight lines, as shown in Fig. 4a. A higher ionic concentration leads to a larger difference for surface charge densities, but a smaller one for zeta potentials, between different pH values.

3. Charge regulation caused by EDL overlap

Eq. (12) is available only when the surface separation is much larger than the screening length. If the surface separations h of interest are comparable to or smaller than the screening length, the EDL interactions may influence the charge regulations at the

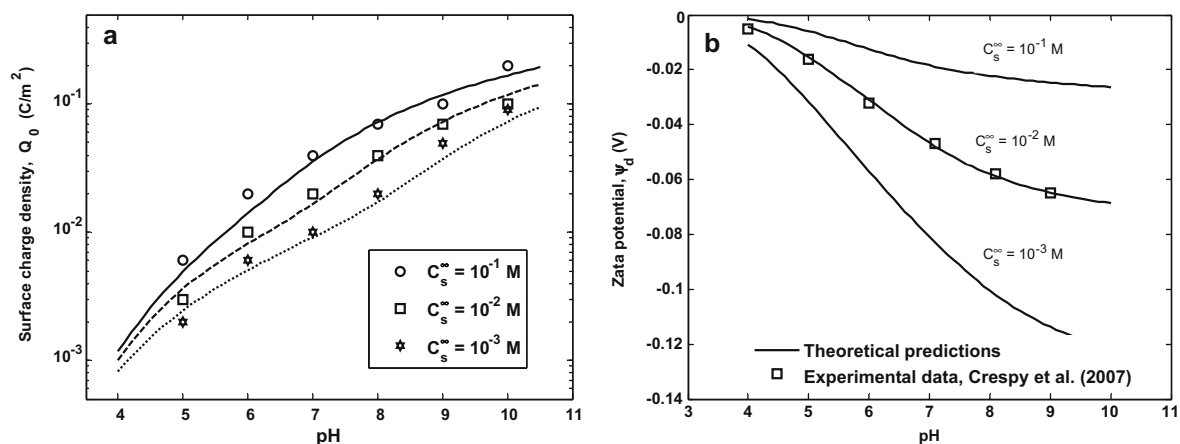


Fig. 2. Comparisons between the predictions by the TLM and the experimental data for the silica surfaces interacting with NaCl solutions. (a) Surface charge density as a function of pH for three different NaCl concentrations. The symbols are the experimental data from Kitamura et al. [26]. (b) Zeta potential as a function of pH for three different NaCl concentrations. The symbols are the experimental data from Crespy et al. [35]. The lines are the predictions by the ETL model. The parameters in the ETL model are $\Gamma^0 = 5$ sites/ nm^2 , $K_{a2}^{int} = 10^{-6.73}$, $K_M^{int} = 10^{-0.25}$, $C_1 = 1.07$ F/ m^2 , and $C_2 = 0.2$ F/ m^2 . The temperature is $T = 298$ K.

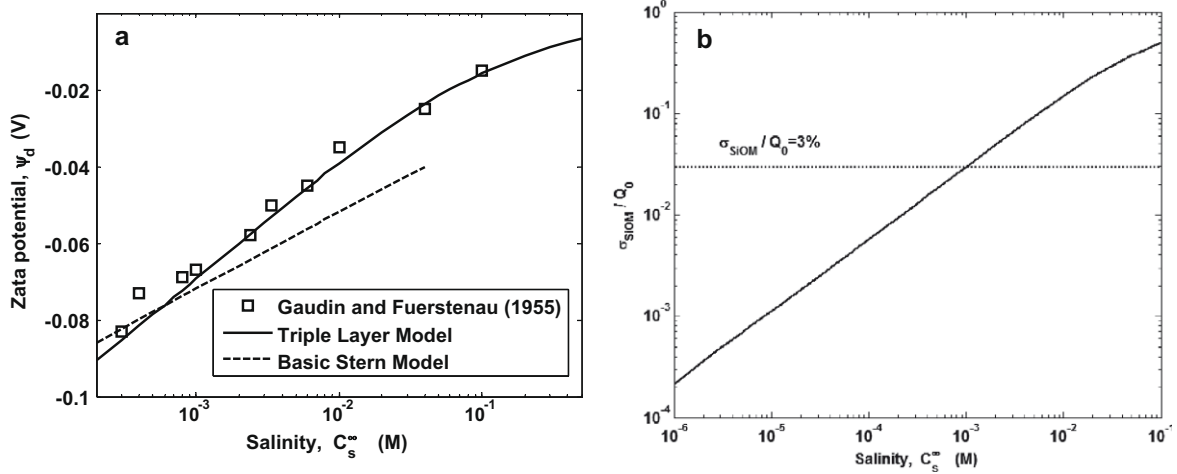


Fig. 3. Effects of salinity on the electrochemical boundaries. (a) The ETL model predictions are compared with the EDL model predictions and the experimental data for different NaCl salinities (data from Refs. [36,37]). (b) The contributions of salt-ion adsorption on the surface charge density for different salinities. The model parameters in ETL are the same as those in Fig. 2. The parameters in the Basic Stern model are $\Gamma = 8$ sites/nm², $pK = 7.5$ and $C = 2.9$ F/m² (data from Ref. [23]). The other working parameters are pH 6.5 and $T = 298$ K.

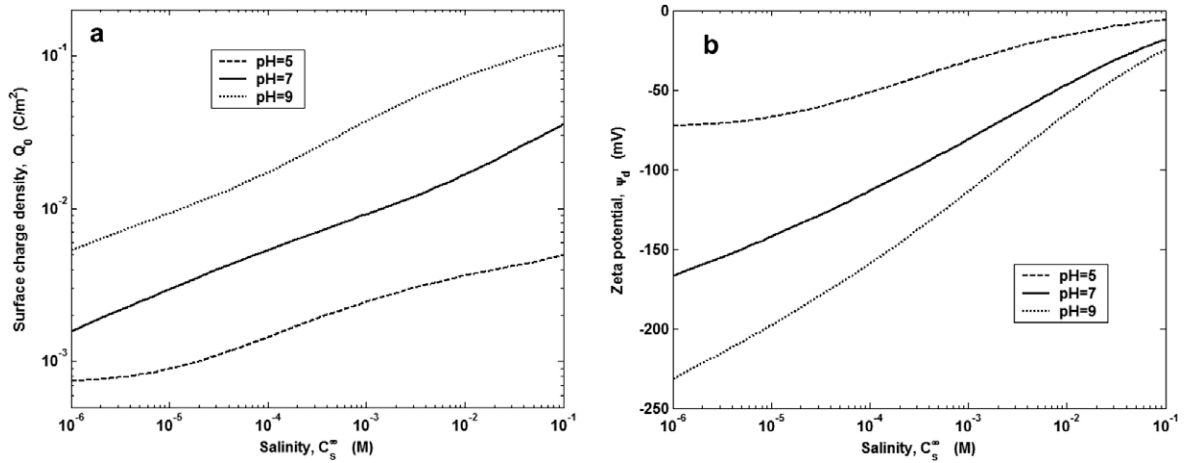


Fig. 4. The surface charge density and the zeta potential of silica surfaces versus salinity for different pH values of NaCl solutions. The surface parameters are as in the previous figures.

surfaces. For electrokinetic transport in a long homogeneously charged channel, at equilibrium state the electric potential gradients along the channel for every species are zero, which leads to the ionic concentrations related to the electric potential by the Boltzmann distribution function [38]:

$$n_i(r) = n_i^m \exp\left(-\frac{ez_i}{kT}(\psi(r) - \psi_m)\right) \quad (17)$$

This relationship has been proved valid through the atomistic simulations for a high ionic concentration even up to almost 1 M [39]. The midline ionic concentration (n_i^m) and the corresponding electric potential (ψ_m) are both unknown at this stage. Under the conditions of electrostatic equilibrium and long homogeneously charged surfaces, the ionic concentration at the midline of the channel is related with that of free far from the surfaces by

$$n_i^m = n_i^\infty \exp\left(-\frac{ez_i}{kT}\psi_m\right), \quad (18)$$

where n_i^∞ denotes the ionic concentration at the reference electric potential $\psi_\infty = 0$. Therefore, the ion distribution in diffuse layer can be expressed as [38]

$$\begin{aligned} n_i(r) &= n_i^\infty \exp\left(-\frac{ez_i}{kT}\psi_m\right) \exp\left(-\frac{ez_i}{kT}(\psi(r) - \psi_m)\right) \\ &= n_i^\infty \exp\left(-\frac{ez_i}{kT}\psi(r)\right). \end{aligned} \quad (19)$$

To build up the relationship between the charge density at outer H layer (Q_d) and the zeta potential $\psi_\infty = 0$ for thick diffuse layers, we have to solve a one-dimensional nonlinear Poisson equation for the electric potential within the diffuse layers.

$$\frac{d^2\psi}{dy^2} = -\frac{1}{\varepsilon} \sum_i z_i n_i^m \exp\left(-\frac{ez_i}{kT}(\psi - \psi_m)\right). \quad (20)$$

Integrate and apply symmetry at the middle of channel,

$$\left.\frac{d\psi}{dy}\right|_{y=m} = 0, \quad (21)$$

and then we obtain

$$\frac{d\psi}{dy} = -\left(\frac{2kT}{\varepsilon}\right)^{1/2} \left(\sum_i n_i^m \left[\exp\left(-\frac{ez_i}{kT}(\psi - \psi_m)\right) - 1\right]\right)^{1/2}. \quad (22)$$

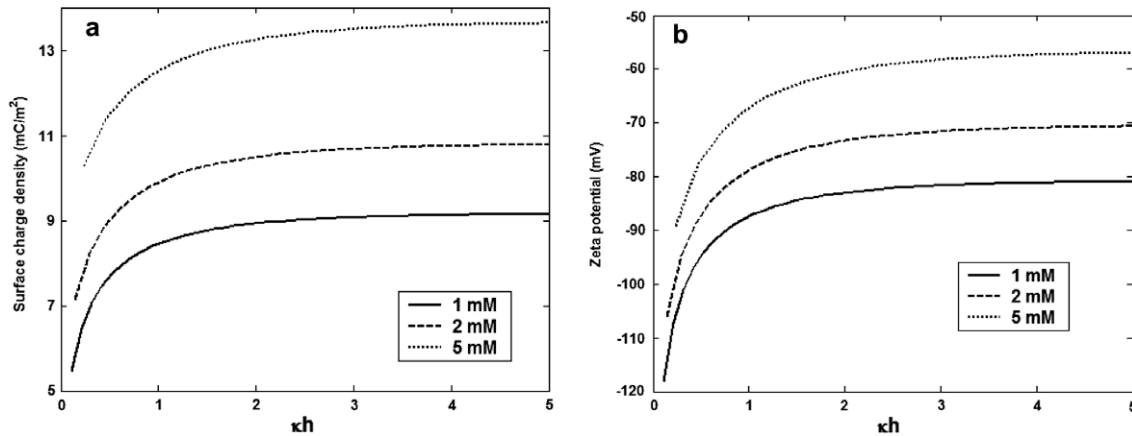


Fig. 5. The surface charge density and the zeta potential of silica surfaces as a function of the channel wall separation. The NaCl solution in the channel is at pH = 7, $T = 298$ K, and $C_s^\infty = 1, 2$ and 5 mM. The channel width (h) varies from 1 to 50 nm. The surface parameters are as in the previous figures.

The classical electrostatics gives

$$Q_d = -\epsilon \frac{d\psi}{dy} \Big|_{y=0} \quad (23)$$

Substitution of Eq. (22) into (23) yields the new relationship between the charge density and the electric potential of the diffuse layer

$$Q_d = 2kT\epsilon^{1/2} \left(\sum_i n_i^m \left[\exp\left(-\frac{ezi}{kT}(\psi_d - \psi_m)\right) - 1 \right] \right)^{1/2} \quad (24)$$

Eq. (24) is a general form, suitable for all kinds of ionic valences. Especially, for the monovalent electrolyte, it has a simplified form as [40]

$$Q_d = \sqrt{8ekTn_s^\infty} \left(\sinh^2\left(\frac{e\psi_d}{2kT}\right) - \sinh^2\left(\frac{e\psi_m}{2kT}\right) \right)^{1/2} \quad (25)$$

Introducing Eq. (25) to replace Eq. (12) into our previous framework yields the coupled governing equations for the surface charge density and zeta potential on silica surfaces even when the double-layers in the channel overlap. The final solutions will be obtained through an iteration process: (i) to solve the old framework (Eqs. (1)–(16)) to get an initial $\psi_d(\zeta)$; (ii) to solve the Poisson equations, Eq. (20), to get a new ψ_m using the ψ_d as boundary conditions; (iii) to solve the new framework (Eqs. (1)–(16) and (25)) with the updated ψ_m to get a new ψ_d ; (iv) repeat (ii) and (iii) until the iteration error reaches the expected tolerance. In our calculations, we set the relative tolerance at 10^{-6} .

Fig. 5 shows the surface charge density and zeta potential changing with the wall separation (κh) in a long parallel-plate silica channel when the channel width (h) varies from 1 to 50 nm. κ^{-1} is defined as the Debye screening length given by $\kappa = \sqrt{2e^2n_s^\infty/\epsilon kT}$. The results indicate that the surface charge density increases with the channel wall separation, similar to the result in Ref. [23] and that the absolute zeta potential decreases with the wall separation. It suggests that the double-layer overlap in channels will decrease the surface charge density but increase the zeta potential on surfaces.

4. Conclusions

We have developed a theoretical framework to calculate the electric charge density and zeta potential on silica surfaces interacting with high-ionic-strength (1 mM to 1 M) solutions in microfluidic and nanofluidic channels. The electrical triple-layer (ETL)

model takes the contributions of the adsorbed metal cations on solid surfaces into account, which increases with the ionic strength. Analytical results indicate that the contribution of the adsorbed metal cations to the total surface charge is not negligible when the salinity is larger than 1 mM. The Basic Stern model in which the adsorption of metal cations is not considered is only valid for low ionic strength ($C_s^\infty < 1$ mM). The regulated charge of silica surfaces in micro- and nanochannels has been derived from an exact relationship between ion density and electric potential when the double-layer overlap occurs. An iteration process is proposed to solve the surface charge density and the zeta potential in very narrow channels. The results indicate that the double-layer overlap (lower κh) in narrow channels will decrease the surface charge density but increase the zeta potential on surfaces.

Acknowledgments

This work is supported by LANL's LDRD Project 20080727PRD2, through the J.R. Oppenheimer Fellowship awarded to M.W. The authors thank Dr. Q. Kang, Dr. M. Bazant and Dr. L. Chen for helpful discussions.

References

- [1] D.Q. Li, Encyclopedia of Microfluidics and Nanofluidics, Springer Verlag, New York, 2008.
- [2] R.B. Schoch, J.Y. Han, P. Renaud, Rev. Mod. Phys. 80 (3) (2008) 839–883.
- [3] D. Stein, M. Kruithof, C. Dekker, Phys. Rev. Lett. 93 (3) (2004) 035901.
- [4] F.H.J. van der Heyden, D. Stein, C. Dekker, Phys. Rev. Lett. 95 (11) (2005) 116104.
- [5] B. Bourlon, J. Wong, C. Miko, L. Forro, M. Bockrath, Nat. Nanotechnol. 2 (2) (2007) 104–107.
- [6] D. Stein, F.H.J. van der Heyden, W.J.A. Koopmans, C. Dekker, Proc. Natl. Acad. Sci. USA 103 (43) (2006) 15853–15858.
- [7] H. Daiguji, P.D. Yang, A. Majumdar, Nano Lett. 4 (1) (2004) 137–142.
- [8] R. Karnik, K. Castelino, R. Fan, P. Yang, A. Majumdar, Nano Lett. 5 (9) (2005) 1638–1642.
- [9] H. Daiguji, P.D. Yang, A.J. Szeri, A. Majumdar, Nano Lett. 4 (12) (2004) 2315–2321.
- [10] S.R. Liu, Q.S. Pu, L. Gao, C. Korzeniewski, C. Matzke, Nano Lett. 5 (7) (2005) 1389–1393.
- [11] F.H.J. van der Heyden, D.J. Bonthuis, D. Stein, C. Meyer, C. Dekker, Nano Lett. 6 (10) (2006) 2232–2237.
- [12] F.H.J. van der Heyden, D.J. Bonthuis, D. Stein, C. Meyer, C. Dekker, Nano Lett. 7 (4) (2007) 1022–1025.
- [13] H.S. White, A. Bund, Langmuir 24 (5) (2008) 2212–2218.
- [14] K.D. Huang, R.J. Yang, Nanotechnology 18 (11) (2007) 115701.
- [15] S. Pennathur, J.G. Santiago, Anal. Chem. 77 (21) (2005) 6772–6781.
- [16] M. Wang, Q. Kang, Anal. Chem. 81 (8) (2009) 2953–2961.
- [17] A.P. Thompson, J. Chem. Phys. 119 (14) (2003) 7503–7511.
- [18] R. Qiao, N.R. Aluru, Phys. Rev. Lett. 92 (19) (2004) 198301/1–4.
- [19] R. Qiao, N.R. Aluru, Appl. Phys. Lett. 86 (14) (2005).
- [20] M. Wang, J. Liu, S. Chen, Mol. Simul. 33 (15) (2007) 1273–1277.

- [21] N. Malikova, V. Marry, J.F. Dufreche, P. Turq, *Curr. Opin. Colloid Interface Sci.* 9 (1–2) (2004) 124–127.
- [22] M. Wang, S. Chen, *J. Colloid Interface Sci.* 314 (1) (2007) 264–273.
- [23] S.H. Behrens, D.G. Grier, *J. Chem. Phys.* 115 (14) (2001) 6716–6721.
- [24] J.A. Davis, R.O. James, J.O. Leckie, *J. Colloid Interface Sci.* 63 (3) (1978) 480–499.
- [25] J.A. Davis, J.O. Leckie, *J. Colloid Interface Sci.* 67 (1) (1978) 90–107.
- [26] A. Kitamura, K. Fujiwara, T. Yamamoto, S. Nishikawa, H. Moriyama, *J. Nucl. Sci. Technol.* 36 (12) (1999) 1167–1175.
- [27] P. Leroy, A. Revil, *J. Colloid Interface Sci.* 270 (2) (2004) 371–380.
- [28] P. Leroy, A. Revil, A. Kemna, P. Cosenza, A. Ghorbani, *J. Colloid Interface Sci.* 321 (1) (2008) 103–117.
- [29] R. Charmas, W. Piasecki, *Langmuir* 12 (22) (1996) 5458–5465.
- [30] R. Charmas, W. Piasecki, W. Rudzinski, *Langmuir* 11 (8) (1995) 3199–3210.
- [31] P. Leroy, A. Revil, S. Altmann, C. Tournassat, *Geochim. Cosmochim. Acta* 71 (5) (2007) 1087–1097.
- [32] T. Hiemstra, J.C.M. Dewit, W.H. Vanriemsdijk, *J. Colloid Interface Sci.* 133 (1) (1989) 105–117.
- [33] J. Persello, in: E. Papirer (Ed.), *Adsorption on Silica Surfaces*, CRC Press, New York, 2000, pp. 297–342.
- [34] M. Wang, *Scientific Computation with MATLAB*, second ed., Publishing House of Electronics Industry, Beijing, 2003.
- [35] A. Crespy, A. Boleve, A. Revil, *J. Colloid Interface Sci.* 305 (1) (2007) 188–194.
- [36] A.M. Gaudin, D.W. Fuerstenau, *Trans. Am. Inst. Min. Metall. Eng.* 202 (1) (1955) 66–72.
- [37] A.M. Gaudin, D.W. Fuerstenau, *Trans. Am. Inst. Min. Metall. Eng.* 202 (10) (1955) 958–962.
- [38] F. Baldessari, J.G. Santiago, *J. Colloid Interface Sci.* 331 (2) (2009) 549.
- [39] M. Wang, S.Y. Chen, *Commun. Comput. Phys.* 3 (5) (2008) 1087–1099.
- [40] J. Goncalves, P. Rousseau-Gueutin, A. Revil, *J. Colloid Interface Sci.* 316 (2007) 92–99.